Dating submarine landslides using the transient response of gas hydrate stability

Alexey Portnov[1*], Kehua You [1], Peter B. Flemings[1], Ann E. Cook[2], Mahdi Heidari[1], Derek E. Sawyer[2], Stefan Bünz[3]

[1] *University of Texas Institute for Geophysics, Austin, Texas, USA*

[2] *School of Earth Sciences, The Ohio State University, Columbus, Ohio, USA*

[3] *Centre for Arctic Gas Hydrate, Environment and Climate (CAGE), University of Tromsø The Arctic University of Norway, Norway.*

ABSTRACT

Submarine landslides are prevalent on the modern-day seafloor, yet an elusive problem is constraining the timing of slope failure. Herein, we present a novel age-dating technique based on perturbations to underlying gas hydrate stability caused by slide-impacted seafloor changes. Using 3D seismic data, we map an irregular bottom simulating reflection (BSR) underneath a submarine landslide in the Orca Basin, Gulf of Mexico. The irregular BSR mimics the pre-slide seafloor geometry rather than the modern bathymetry. Therefore, we suggest that the gas hydrate stability zone (GHSZ) is still adjusting to the post-slide sediment temperature. We apply transient conductive heat flow modeling to constrain the response of the GHSZ to the slope failure, which yields a most likely age of ~8 ka demonstrating that gas hydrate can respond to landslides even on the multi-millennial timescales. We further provide a generalized analytical solution that can be used to remotely date submarine slides in absence of traditional dating techniques.

INTRODUCTION

Submarine slope failures are hazardous mass transport events that can mobilize tens and hundreds of cubic kilometers of sediments in a matter of hours (Masson et al., 2006; Locat and Lee, 2011). Submarine slides can cause destructive tsunamis and damage to costly seabed infrastructure, yet the causes of these events are often unknown (Harbitz et al., 2006; Carter et al., 2014; Talling et al., 2014). Tectonic activity, excess pore pressure, and development of weak layers are important mechanisms that may reactivate during certain geologic cycles and cause slope instability (Hampton et al., 1996; Locat and Lee, 2011). Therefore, defining the age of a landslide can help constrain potential origin, triggers and repeatability of slope failures (Urlaub et al., 2013; Pope et al., 2015). Slide age can be determined using various sediment dating approaches, pore water chemistry and modeling; however, this is often limited by the availability of sediment cores (Henkel et al., 2011; Urlaub et al., 2013; Pope et al., 2015; Luo et al., 2020). Our study uses a new approach that does not require sediment core data, instead, we use bottom simulating reflections (BSRs) mapped in seismic data to determine a landslide age.

BSRs are commonly observed in reflection seismic data and are associated with natural gas hydrate – solid compounds of water and gas existing within the gas hydrate stability zone (GHSZ) (Kvenvolden and Lorenson, 2001; Haacke et al., 2007). The base of the GHSZ is a sensitive interface controlled by a combination of four factors: pressure, temperature, gas composition, and pore water salinity (Kvenvolden, 1993; Kvenvolden and Lorenson, 2001). Typically, in a steady-state system, the four factors remain regionally uniform and the BSR parallels the seafloor deepening with increasing water depth (Shipley et al., 1979). Non-steady-state BSRs have also been observed and attributed to sea level oscillations, Quaternary climate changes (e.g. Musgrave et al., 2006; Davies et al., 2017) or subseafloor fluid flow (e.g. Smith et al., 2014). Here, we analyze a non-steady-state BSR that deviates from the modern bathymetry due to slide-induced temperature perturbations in the sediments. We determine the age of the submarine landslide based on the deviation of the modern BSR from its steady-state depth using the modeled pre-slide bathymetry, the post-slide sediment temperature and stability behavior of methane hydrate.

GEOLOGIC SETTING

The Orca Basin in the Gulf of Mexico is a salt-withdrawal minibasin (1600-2600 m water depth) marked by prominent escarpments and rugged topography resulting from slump deposits produced by multiple submarine slide events (Pilcher and Blumstein, 2007; Sawyer et al., 2019) (Figure 1A, B). Our study area is located at the southern flank of the Orca Basin where a sharp ~

90 meters tall seafloor escarpment marks the head of a submarine slide described in Sawyer et al (2019) (Figure 1A). Sawyer et al (2019) also reported an accumulation of MTDs below a brine pool at the basin floor (Figure 1A, B). The BSR was previously mapped in Hillman et al (2017) and further analyzed in this study over an area of ~44.3 km^2 (Figure 1C, D).

IRREGULAR BSR IN THE ORCA BASIN

In the depth-migrated 3D seismic data, we observe multiple distinct reversed-polarity BSRs that crosscut stratigraphy (Figure 1D, 2A, supplemental information). The BSRs are located at a wide depth range of 230-1130 meters below seafloor (mbsf) (Figure 1C), which is surprising given that they are typically subparallel to the seafloor. The irregular BSR configuration is especially well-observed along seismic section c-d extending across the southern rim and slope of the Orca Basin (Figure 2A, B).

There are two reasonable explanations for the irregular BSR. First, the shallower BSR could be caused by the higher sediment temperature over the heat-conductive salt body, which would drive the base of the GHSZ upward (Hornbach et al., 2005; Portnov et al., 2020). The geothermal gradients required to explain the depths of the observed BSR along the profile c-d would show a significant increase from 16.3 °C/km downslope to as high as 43 °C/km above the salt summit (Figure 2A, supplemental information). Second, the irregular BSR may be explained by the effect of the slide, as the BSR is in a striking agreement with the reconstructed pre-slide bathymetry of the Orca Basin southern rim (Figure 2A, B, supplemental information). The observed BSR lies at an approximately constant depth below the reconstructed pre-slide seafloor both, within the slide escarpment upslope and downslope, where the pre-slide seafloor submerges along the base of the MTD (Figure 1C inset, Figure 2A, B). This suggests the base of the GHSZ in the Orca Basin may still closely reflect the pre-slide seafloor configuration.

To understand the temperature effect of the salt body on the observed BSR shape, we run a 2D conductive heat flow model along profile c-d (Figure 1) (supplemental information). We then correlate the observed BSR with the modeled response of the GHSZ to the slide-induced temperature perturbations and define the age of the slope failure.

RESULTS AND DISCUSSION

The geothermal gradient predicted by the 2D heat flow model assumes average regional gradient of 25.5 °C/km derived using steady-state BSR depths (Figure 2A, supplementary information). Over the salt body, the model predicts 30 °C/km, and it gradually decreases to the average regional 25.5 °C/km northward from the salt summit (supplemental information, Figure 2A). However, these variations are insufficient to explain the shape of the irregular BSR, which requires geothermal gradients increasing from 16.3 °C/km downslope to as high as 43 °C/km above salt (Figure 2A).

To analyze the effect of the slide on the BSR, profile c-d can be divided into two areas: 1) the upslope area where the removal of the overburden is cooling the shallow sediments and drives the base of GHSZ down (Figure 2B), 2) the downslope area where the warming effect due to the deposition of the MTD drives the base of GHSZ upward. In the areas outside of the MTD and slide escarpment, the GHSZ is assumed steady-state (Figure 2B). Based on the 1D heat flow modeling, we define the transient temperature changes in the sediment column (time-temperature profiles) after the slide for the upslope and downslope locations (supplemental information). Finally, to define the age of the slide event in the Orca Basin, we find the crossover of the methane phase boundary curve, the observed BSR depth, and the corresponding time-temperature profile (insets of Figure 2B).

Age of the Orca Submarine Slide

Given the 30 °C/km steady-state geothermal gradient at the upslope location, the pre-slide temperature at the level of the modern seafloor (~220 meters below the pre-slide seafloor) was 10.7 °C (Figure 3A). After the instantaneous ~220-meter seafloor drop caused by the slide, these warmer sediments were exposed to cooler bottom waters with a temperature 4.2 °C (Herring, 2010)(Figure 3A). Over time, the temperature within the subseafloor sediments gradually cools to adjust to the new boundary condition as shown by the time-temperature profiles (Figure 3A). Based on the steady-state geothermal gradient, the pre-slide BSR would have been at ~245 meters below the modern seafloor (Figure 3A), and it will reach its post-slide steady-state depth at ~505 mbsf, ~200 kyr after the slide event. Figure 3A shows that the intersection of the modern BSR (~342 mbsf) and methane phase boundary curve corresponds to the ~8.0 kyr time-temperature profile defining the age of the slide (red curve in Figure 3A). To verify this result, we run our model at a second upslope location (Figure 2A, B) and acquire a similar age of ~7.5 kyr. Difference between the two upslope locations may result from high sensitivity of our model to input parameters, as explained below.

The Orca landslide age estimates may be affected by factors that control gas hydrate stability, such as the presence of heavy hydrocarbons that would result in younger modeled slide age (for reference, Figure 3A shows a 5% ethane admixture, decreasing the slide age by several kyrs). Thermogenic gas presence at the Orca location, however, is unlikely based on the mud log gas chromatography and seismic data (supplementary information).

Below the slide escarpments (i.e. the upslope location), the deepening GHSZ entraps the underlying gas, which forms hydrate (Figure 2B). It is an exothermic process accompanied by heat release, which may slow the cooling trend and increase the modeled slide age. Figure 3B shows an extreme scenario assuming a 150-m thick gas column below the GHSZ and a 50 m-thick interval with 50% gas hydrate saturation above, which results in the older modeled slide age (supplementary information). Such scenario is not supported by the seismic and log data, yet any effect of hydrate formation would indicate that 8 kyr is the youngest age for the Orca landslide.

At the downslope location, we run a similar model with a 400-meter thick sediment mass added to the top of the pre-slide seafloor to simulate the deposition of the MTD (Figure 2B, supplementary information). The modeled age acquired at the downslope location is ~14 ka. We consider the upslope age estimate of ~8 ka more accurate for several reasons. First, sediment removal at the upslope location was likely a single fast-moving event (Sawyer et al., 2019). In contrast, the MTD at the downslope location may be an amalgamation of several landslides (Sawyer et al., 2019), and the temperature profiles may record a number of slides, some older than the most recent event released at the upslope location. Second, the thermal signal propagates faster between the pre-slide and modern BSR upslope than at the deeper BSR downslope, resulting in the wider-spaced time-temperature profiles and better age resolution. Finally, the Orca landslide was hypothesized to produce a tsunami wave in the 7.9-8.5 ka-old brine pool (Sawyer et al., 2019) (Figure 1A, 2), indicating the landslide was younger or synchronous in time.

Generalized Approach to Submarine Slide Dating Using BSRs

There are several examples where published seismic data show irregular BSRs below the landslide-impacted seafloor: the Cape Fear slide complex offshore the US East Coast (Hill et al., 2019), offshore Oregon, USA (Lenz et al., 2018), the Brunei slide offshore Brunei (Gee et al., 2007), the Hinlopen megaslide (Geissler et al., 2016) and multiple landslides on the

Hikurangi margin (Henrys et al., 2003; Watson et al., 2020). Given these locations and constantly expanding seismic databases worldwide, we have developed an analytical method that can be used as a quick-look slide age (t_{slide}, s) tool in similar systems. The model uses the modern BSR depth (Z_{bsr}, m) below slide escarpments (similar to the Orca upslope location) with a known temperature at the BSR depth (T_{bsr})(Figure 3A, 4) (see supplemental information). The parameter $\frac{T_{bsr}-T_{z,o}}{T_{s,1}-T_{s,o}}$ is used to quantify the fractional heat dissipation after the slide, with a value of zero referring to the initial condition immediately after the slide and a value of 1 referring to the post-slide steady state (Figure 4). The plots of the fractional heat dissipation ($\frac{T_{bsr}-T_{z,o}}{T_{s,1}-T_{s,o}}$) versus the dimensionless time ($\frac{\kappa t}{z^2 bsr}$) all fall into one curve at different locations with different water depths, temperature gradients, thermal diffusivities, BSR temperatures and/or landslide thicknesses (Figure 4: red curve). This means that the age of a submarine landslide t_{slide} can be estimated from the diagram shown in Figure 4 with computable parameters (T_{bsr}, $T_{z,o}$, $T_{s,1}, T_{s,0}, \kappa$). To easily derive the input parameters and perform the analytical solution, we developed a desktop app for quick-look submarine landslide dating (supplementary information).

The analytical solution for the Orca upslope location using 30±1 °C/km geothermal gradient dates the slide to ~7.5±2 ka (Figure 4), close to our numerical modeling results (7.5-8.0 ka). We further validate the analytical solution at the Storegga landslide with well-constraint input parameters, which has been previously dated to ~8.1±0.25 ka (Haflidason et al., 2005). Our analytical solution produces a slide age of ~8.1 ka, which is similar to the existing estimate (supplemental information).

Sensitivity of landslide dating

In this approach the predicted age is highly sensitive to even small changes in input parameters. Generally, slide age prediction is more accurate in areas with higher heat flow and for larger and younger slides (<~15 ka). For example, at the Orca location, a ±1 °C/km change in the geothermal gradient results in a ~±2 kyr of age uncertainty (Figure 4, supplementary information). Furthermore, an uncertainty of ±10 m in the slide thickness and ±5 m in the BSR depth result in ~ ±0.9 kyr uncertainty in slide age (supplemental information). Such sensitivity is higher compared to the traditional dating methods. Nonetheless, our method provides a novel approach to remotely predict a slide age without directly sampling the location.

CONCLUSIONS

We estimate the age of the submarine landslide on the southern bank of the Orca Basin to be ~8.0 ka based on the modern BSR depth in seismic data coupled with numerical heat flow models. We also provide an analytical solution for quick-look age estimates for submarine slide where seismic and temperature data are available. Our study shows that the Orca and similar gas hydrate systems expand below the slide escarpments and dissociate below the MTDs. Finally, we find such transformations can be still ongoing thousands of years after the slope failures indicating long-lasting dynamic behavior of slide-impacted gas hydrate systems.

ACKNOWLEDGEMENTS

This work is supported by U.S. Department of Energy under contract DE-FE0023919. For our seismic interpretation we used a seismic volume provided by WesternGeco. We thank Manasij Santra for his help with salt mapping.

FIGURE CAPTIONS

Figure 1. A) Seafloor bathymetry (Kramer and Shedd, 2017) showing the submarine slide escarpment (white dotted line) in the Orca Basin, Gulf of Mexico. B) Reconstructed pre-slide bathymetry (see supplemental information). C) Colored areas in the big panel show the BSR extent and depth (mbsl). Pink line outlines the slide escarpment over the gray shaded bathymetry surface. The two panels on the right show the highly variable BSR depth below the modern seafloor (upper) and more coherent BSR depth below the reconstructed pre-slide seafloor (lower). D) Seismic cross section a-b shows three industry wells with plotted gamma ray (green) and resistivity (red) logs. Possible hydrate intervals are evident from the high-resistivity intervals above the BSR in the wells WR143-001 and WR143-003.

Figure 2. A) Seismic cross-section c-d showing the BSR (blue arrows), which is not parallel to the modern seafloor, but strikingly parallel to the reconstructed pre-slide seafloor (red dotted line). Geothermal gradients required to explain the depth of the bottom simulating reflection using the pre-slide seafloor (red) show better consistency than those calculated using the BSR and modern seafloor depths (green); the left inset shows steady-state BSR locations (stars) outside of the slide escarpment (pink line) and away from the shallow salt (colored surface) selected for calculation of the regional average geothermal gradient (25.5 °C/km). B) Interpreted seismic section c-d showing the upslope and downslope locations selected for modeling analyses. Elements of the slide-gas hydrate system are labeled. Insets show schematic adjustment of the temperature field after the slope failure leading to the reciprocal BSR shifts. SF-seafloor; PSF – pre-slide seafloor; T-temperature; D-depth; $t_{0\text{-}n}$ -time-temperature profiles.

Figure 3. Transient 1D heat flow modeling at the primary upslope location showing the time-temperature profiles after the removal of overburden assuming no gas hydrate formation (A) and with gas hydrate formation (B). Intersection of the red time-temperature profile, modern

BSR and methane hydrate phase boundary in (A) indicates the most likely ~8.0 kyr age of the Orca landslide (see supplemental information).

Figure 4. The analytical solution, which estimates submarine slide age using temperature change at the depths of the modern BSR, similar to the upslope location at Orca. The slide age (t_{slide}) is calculated by acquiring the fractional dissipation (where $T_{s,0}$ and $T_{s,1}$ are the temperature at the modern seafloor level before and after the slide, respectively (°C); $T_{z,0}$ is the initial temperature at the depth of the modern BSR (°C); T_{bsr} can be derived using the modern BSR depth and hydrate phase boundary diagram. z_{bsr} is the modern BSR depth; κ is the average thermal diffusivity of the subseafloor sediment (supplemental information).

REFERENCES

Carter, L.R., Gavey, R., Talling, P.J., and Liu, J.T., 2014, Insights into submarine geohazards from breaks in subsea telecommunication cables: Oceanography, v. 27, p. 58–67.

Davies, R.J., Maqueda, M.Á.M., Li, A., and Ganopolski, A., 2017, Millennial-scale shifts in the methane hydrate stability zone due to Quaternary climate change: Geology, v. 45, p. 1027–1030, doi:10.1130/G39611.1.

Gee, M.J.R., Uy, H.S., Warren, J., Morley, C.K., and Lambiase, J.J., 2007, The Brunei slide: A giant submarine landslide on the North West Borneo Margin revealed by 3D seismic data: Marine Geology, v. 246, p. 9–23, doi:10.1016/J.MARGEO.2007.07.009.

Geissler, W.H., Gebhardt, A.C., Gross, F., Wollenburg, J., Jensen, L., Schmidt-Aursch, M.C., Krastel, S., Elger, J., and Osti, G., 2016, Arctic megaslide at presumed rest: Scientific

Reports, v. 6, p. 38529, doi:10.1038/srep38529 http://www.nature.com/articles/srep38529#supplementary-information.

Haacke, R.R., Westbrook, G.K., and Hyndman, R.D., 2007, Gas hydrate, fluid flow and free gas: Formation of the bottom-simulating reflector: Earth and Planetary Science Letters, v. 261, p. 407–420, doi:10.1016/j.epsl.2007.07.008.

Haflidason, H., Lien, R., Sejrup, H.P., Forsberg, C.F., and Bryn, P., 2005, The dating and morphometry of the Storegga Slide: Marine and Petroleum Geology, v. 22, p. 123–136, doi:10.1016/J.MARPETGEO.2004.10.008.

Hampton, M.A., Lee, H.J., and Locat, J., 1996, Submarine landslides: Reviews of Geophysics, v. 34, p. 33–59, doi:10.1029/95rg03287.

Harbitz, C.B., Lovholt, F., Pedersen, G., Glimsdal, S., and Masson, D.G., 2006, Mechanisms of tsunami generation by submarine landslides - a short review: Norwegian Journal of Geology, v. 86, p. 255–264, http://nora.nerc.ac.uk/142982/.

Henkel, S. et al., 2011, An interdisciplinary investigation of a recent submarine mass transport deposit at the continental margin off Uruguay: Geochemistry, Geophysics, Geosystems, v. 12, doi:https://doi.org/10.1029/2011GC003669.

Henrys, S.A., Ellis, S., and Uruski, C., 2003, Conductive heat flow variations from bottom-simulating reflectors on the Hikurangi margin, New Zealand: Geophysical Research Letters, v. 30, doi:10.1029/2002GL015772.

Herring, J., 2010, Gulf of Mexico Hydrographic Climatology and Method of Synthesizing Subsurface Profiles From the Satellite Sea Surface Height Anomaly:, https://geo.gcoos.org/data/ssha/ssha_ts_proflies.pdf.

Hill, J.C., Brothers, D.S., Hornbach, M.J., Sawyer, D.E., Shillington, D.J., and Bécel, A., 2019, Subsurface controls on the development of the Cape Fear Slide Complex, central US Atlantic Margin: Geological Society, London, Special Publications, v. 477, p. 169–181, doi:10.1144/SP477.17.

Hillman, J.I.T., Cook, A.E., Sawyer, D.E., Küçük, H.M., and Goldberg, D.S., 2017, The character and amplitude of 'discontinuous' bottom-simulating reflections in marine seismic data: Earth and Planetary Science Letters, v. 459, doi:10.1016/j.epsl.2016.10.058.

Hornbach, M.J., Ruppel, C., Saffer, D.M., Van Dover, C.L., and Holbrook, W.S., 2005, Coupled geophysical constraints on heat flow and fluid flux at a salt diapir: Geophysical Research Letters, v. 32, doi:10.1029/2005gl024862.

Kramer, K. V, and Shedd, W.W., 2017, A 1.4-billion-pixel map of the Gulf of Mexico seafloor: Earth and Space Science News, v. 98.

Kvenvolden, K.A., 1993, Gas hydrates-geological perspective and global change: Reviews of Geophysics, v. 31, p. 173–187, doi:10.1029/93RG00268.

Kvenvolden, K.A., and Lorenson, T.D., 2001, The Global Occurrence of Natural Gas Hydrate: Natural Gas Hydrates: Occurrence, Distribution, and Detection, p. 3–18, doi:10.1029/GM124p0003.

Lenz, B.L., Sawyer, D.E., Phrampus, B., Davenport, K., and Long, A., 2018, Seismic Imaging of Seafloor Deformation Induced by Impact from Large Submarine Landslide Blocks, Offshore Oregon: Geosciences 2019, Vol. 9, Page 10, v. 9, p. 10, doi:10.3390/GEOSCIENCES9010010.

Locat, J., and Lee, H.J., 2011, Submarine landslides: advances and challenges: https://doi.org/10.1139/t01-089, v. 39, p. 193–212, doi:10.1139/T01-089.

Luo, M., Torres, M.E., Kasten, S., and Mountjoy, J.J., 2020, Constraining the Age and Evolution of the Tuaheni Landslide Complex, Hikurangi Margin, New Zealand, Using Pore-Water Geochemistry and Numerical Modeling: Geophysical Research Letters, v. 47, p. e2020GL087243, doi:https://doi.org/10.1029/2020GL087243.

Masson, D.G., Harbitz, C.B., Wynn, R.B., Pedersen, G., and Løvholt, F., 2006, Submarine landslides: Processes, triggers and hazard prediction: Philosophical Transactions of the Royal Society A: Mathematical, Physical and Engineering Sciences, v. 364, p. 2009–2039, doi:10.1098/rsta.2006.1810.

Musgrave, R.J., Bangs, N.L., Larrasoaña, J.C., Gràcia, E., Hollamby, J.A., and Vega, M.E., 2006, Rise of the base of the gas hydrate zone since the last glacial recorded by rock magnetism: Geology, v. 34, p. 117–120, doi:10.1130/G22008.1.

Pilcher, R.S., and Blumstein, R.D., 2007, Brine volume and salt dissolution rates in Orca Basin, northeast Gulf of Mexico: AAPG Bulletin, v. 91, p. 823–833, doi:10.1306/12180606049.

Pope, E.L., Talling, P.J., Urlaub, M., Hunt, J.E., Clare, M.A., and Challenor, P., 2015, Are large submarine landslides temporally random or do uncertainties in available age constraints make it impossible to tell? Marine Geology, v. 369, p. 19–33, doi:10.1016/J.MARGEO.2015.07.002.

Portnov, A., Cook, A.E., Heidari, M., Sawyer, D.E., Santra, M., and Nikolinakou, M., 2020, Salt-driven evolution of a gas hydrate reservoir in Green Canyon, Gulf of Mexico: AAPG Bulletin, v. 104, p. 1903–1919, doi:10.1306/10151818125.

Sawyer, D.E., Mason, R.A., Cook, A.E., and Portnov, A., 2019, Submarine Landslides Induce Massive Waves in Subsea Brine Pools: Scientific Reports, v. 9, doi:10.1038/s41598-018-36781-7.

Shipley, T.H., Houston, M.H., Buffler, R.T., Shaub, F.J., McMillen, K.J., Ladd, J.W., and Worzel, J.L., 1979, Seismic Evidence for Widespread Possible Gas Hydrate Horizons on Continental Slopes and Rises: AAPG Bulletin, v. 63, p. 2204–2213, doi:10.1306/2F91890A-16CE-11D7-8645000102C1865D.

Smith, A.J., Mienert, J., Bünz, S., and Greinert, J., 2014, Thermogenic methane injection via bubble transport into the upper Arctic Ocean from the hydrate-charged Vestnesa Ridge, Svalbard: Geochemistry, Geophysics, Geosystems, v. 15, p. 1945–1959, doi:10.1002/2013GC005179.

Talling, P.J., Clare, M., Urlaub, M., Pope, E., Hunt, J.E., and Watt, S.F.L., 2014, Large submarine landslides on continental slopes: Geohazards, methane release, and climate change: Oceanography, v. 27, p. 32–45, doi:10.5670/OCEANOG.2014.38.

Urlaub, M., Talling, P.J., and Masson, D.G., 2013, Timing and frequency of large submarine landslides: Implications for understanding triggers and future geohazard: Quaternary Science Reviews, v. 72, p. 63–82, doi:10.1016/j.quascirev.2013.04.020.

Watson, S.J., Mountjoy, J.J., and Crutchley, G.J., 2020, Tectonic and geomorphic controls on the distribution of submarine landslides across active and passive margins, eastern New Zealand: Geological Society Special Publication, v. 500, p. 477–494, doi:10.1144/SP500-

2019-165.

Author contributions

A.P. developed the idea that led to the paper, interpreted seismic data, and designed the figures. K.Y. and A.P. applied 1D transient heat flow and gas hydrate stability zone modeling. M.H. provided 2D conductive heat flow model. D.E.S. provided the porosity profiles. P.B.F., A.E.C. and K.Y. advised on the study’s scope and conception. S.B. Provided data and advise on the Storegga Landslide. A.P. wrote the original manuscript, all authors contributed to the editing of the manuscript.

Competing interests

The authors declare no competing interests

Supplemental information for the manuscript entitled

Dating submarine landslides using the transient response of gas hydrate stability

Alexey Portnov[1*], Kehua You [1], Peter B. Flemings[1], Ann E. Cook[2], Mahdi Heidari[1], Derek E. Sawyer[2], Stefan Bünz[3]

[1] *University of Texas Institute for Geophysics, Austin, Texas, USA*

[2] *School of Earth Sciences, The Ohio State University, Columbus, Ohio, USA*

[3] *Centre for Arctic Gas Hydrate, Environment and Climate (CAGE), University of Tromsø The Arctic University of Norway, Norway.*

1. Methods

3D seismic data and pre-slide seafloor reconstruction

The seafloor, BSR, and salt surface are mapped in the 3D-seismic data sampled to 4.8 m. We use 3D seismic data, which was originally converted from time to depth by WesternGeco. The seismic data provide accurate depths within the GHSZ (our target interval), which is supported by a good correlation between the depths of major seismic horizons (e.g. seafloor and salt top) and corresponding responses in resistivity and gamma ray well logs available in the study area (Figure 1D, main text). The frequency of the processed seismic data ranges from 5-55 Hz providing ~7-9 m vertical resolution at the BSR level.

We use the seafloor seismic reflection to reconstruct the pre-slide seafloor geometry and infer the base of the GHSZ before the slide event following the previously used approach at other submarine landslides (Bondevik et al., 2005; Haflidason et al., 2005; Vanneste et al., 2011). For this reconstruction, we use manual and automatic interpolation of the bathymetric contours from the seafloor surface surrounding each headwall scarp: 1) remove bathymetry data from within the slide escarpment (headwall and sidewalls) 2) iteratively use automatic gridding algorithm (moving average) and manual correction to assure the optimal pre-slide seafloor geometry 3) tune the pre-slide seafloor along the modeling 2D profile. The approach provides a reasonable estimate of the change in water depth after the slide event and with it, the total volume of the slide (Figure 1B, Figure 2A, B). Under the basin floor, we extend the pre-slide seafloor surface along the base of the MTD marked by a distinct trough-leading reflector indicating more consolidated slide sediments onlapping the ancient seafloor (Figure 2A, B).

Gas hydrate phase boundary and geothermal gradients

The gas hydrate phase boundary was estimated assuming 100% methane concentration, 3.5% NaCl, and hydrostatic pressure (Sloan and Koh, 2008). The assumption of pure methane gas is supported by the seismic data showing no deep-rooted migration pathways that could source heavier hydrocarbons towards the base of the GHSZ. There are only a few gas chromatographic measurements available from the mud logs right above the salt body (~1000-1200 m below the base of GHSZ). Two wells (WR143-001 and WR98-001) show methane and only ~0.05 and 0.2 % ethane in total gas composition respectively. It is possible that methane concentration becomes even higher immediately below the GHSZ as has been observed in the Gulf of Mexico (Portnov et al., 2019). Single supra-salt measurement in the well WR143-003 showed ~5% ethane, which we use as an extreme scenario shown in Figure 3, main text. To estimate the mean geothermal gradient, we apply linear temperature approximation between the seafloor and the BSR, using a bottom water temperature of 4.2 °C (Herring, 2010), the BSR depth, and the methane hydrate phase boundary diagram (Sloan and Koh, 2008).

2D conductive heat flow model

2D plane-strain finite-element conductive heat flow model is used to estimate the effect of the salt body on the geothermal gradients along seismic section c-d (Supplementary Figure 1). The 2D plane-strain model assumes that the salt diapir geometry and the sea floor topography don't change in the dimension perpendicular to the studied section, and as a result, there is no heat flow perpendicular to the studied section. The model domain is 14 km deep and 17 km wide with constant basal heat flow (Supplementary Figure 1A, 2). The geometry of the salt body and the seabed topography are obtained from the 3D seismic data (Supplementary Figure 1A).

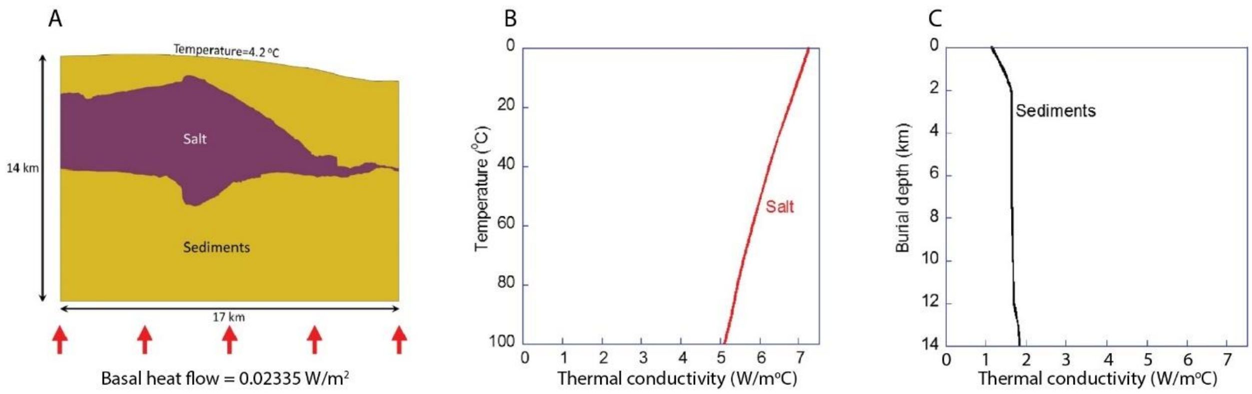

Supplementary Figure 1 A) 2D steady-state conductive heat flow model configuration used to analyze the effect of the salt body on the sediment temperature and estimate the local geothermal gradients for the transient 1D heat flow modeling B) Thermal conductivity of salt, which varies with temperature C) Thermal conductivity of sediments, which is porosity-dependent and varies with depth (Christie and Nagihara, 2016).

Heat flow in the model occurs only through conduction, which assumes that heat advection due to pore fluid migration is negligible. The radiogenic heat, which produces heat in addition to the basal heat flow, is absent in salt and 1.0E-6 W/m^3 in the sediments (Christie and Nagihara, 2016). The boundary conditions include a uniform temperature of 4.2 °C at the seafloor, no heat flow at the side boundaries, and a uniform basal heat flow of 0.0234 W/m^2 (Supplementary Figure 1A). The basal heat flow is constrained by the seafloor temperature and regional average geothermal gradient of 25.5 °C/km (see inset Figure 2, main text). The thermal conductivity of salt varies with temperature (Mello et al., 1995), ranging from ~5 W/m °C at the base of the salt body to ~7 W/m °C at the top of the model (Supplementary Figure 1B). The thermal conductivity of sediments (~1 to 2 W/m °C) depends on the porosity and the mineralogy, and the porosity decreases with depth according to observations in shallow marine sediments in the Gulf of Mexico (Christie and Nagihara, 2016) (Supplementary Figure 1C). The model is built using the commercial finite element code Abaqus 6.16 (Dassault Systems).

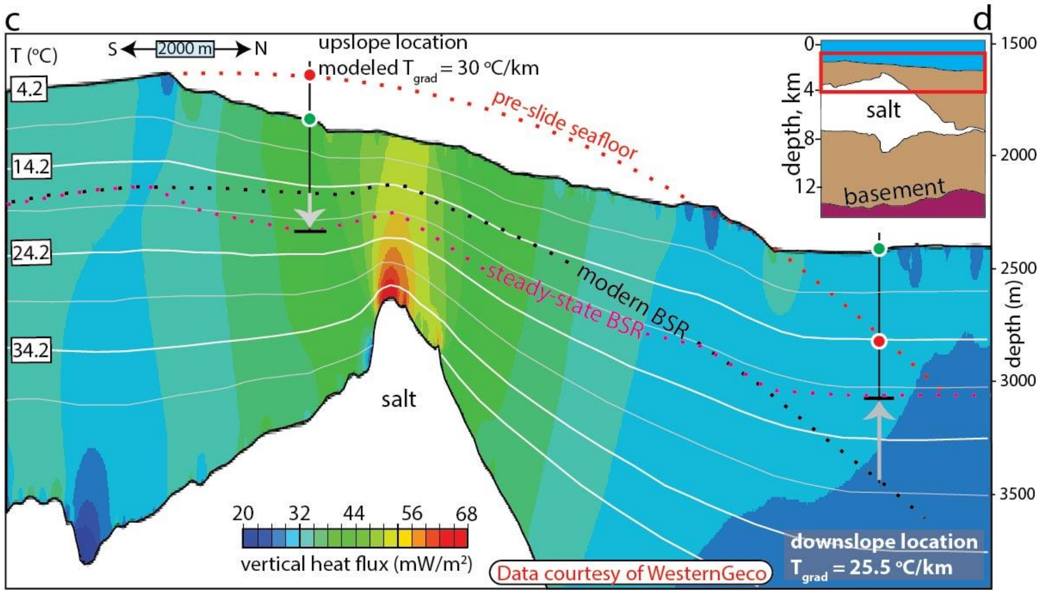

Supplementary Figure 2. Two-dimensional steady-state conductive heat flow model.

The model predicts an elevated geothermal gradient over salt (~30°C/km) and regional average geothermal gradient below the MTD (~25.5°C/km), which is however insufficient to explain the observed shift in the BSR in the Orca Basin (Figure 2A, main text). We use the gradients at the upslope (30°C/km) and downslope (25.5°C/km) locations for our one-dimensional simulations (Figure 3, main text). Moreover, the 2D heat flow model predicts where the base of GHSZ would be at steady-state, and indicates that the sediments are still undergoing the residual post-slide temperature adjustment (Supplementary Figure 2).

Transient 1D heat flow modeling

We use a numerical model (You and Flemings, 2018) with a vertical grid size of 10 m to simulate the transient temperature change below the slide-impacted seafloor upon an instantaneous temperature change at the seafloor. At time 0, we set the upper boundary condition (temperature at the seafloor) to 4.2 °C and keep it constant with time. The base of the model is at the depth that is ~5 times the depth of the BSR, where there is a constant geothermal heat supply that correlates with the local geothermal gradients predicted by the 2D heat flow model: 30 °C/km at the upslope location and 25.5 °C/km at the downslope location (Supplementary Figure 2). In the first scenario, we don't consider gas hydrate formation assuming that the pores are fully saturated with water. The temperature is calculated from the energy conservation equation:

$$\frac{\partial[C_{bulk}T]}{\partial t} - \frac{\partial}{\partial z}\left[\lambda_{bulk}\frac{\partial T}{\partial z}\right] = 0, \quad (1)$$

where t is time (s); z is depth below the seafloor (m); T is temperature (°C); C_{bulk} is the bulk heat capacity (J kg^{-1} ^{o}C^{-1}) of the sediment; λ_{bulk} is the bulk thermal conductivity (W m^{-1} ^{o}C^{-1}). C_{bulk} and λ_{bulk} increase with depth as the porosity decreases (Supplementary Figure 3).

In the second scenario, we consider the latent heat effect of gas hydrate formation and dissociation, and we use a multi-phase (liquid water, methane hydrate, gas) flow and multi-component (water, methane and salt) reactive transport numerical model developed and described in details in You and Flemings (2018). We then derive the temperature profiles at certain times (time-temperature profiles) after the slide for both locations (Figure 3B, main text).

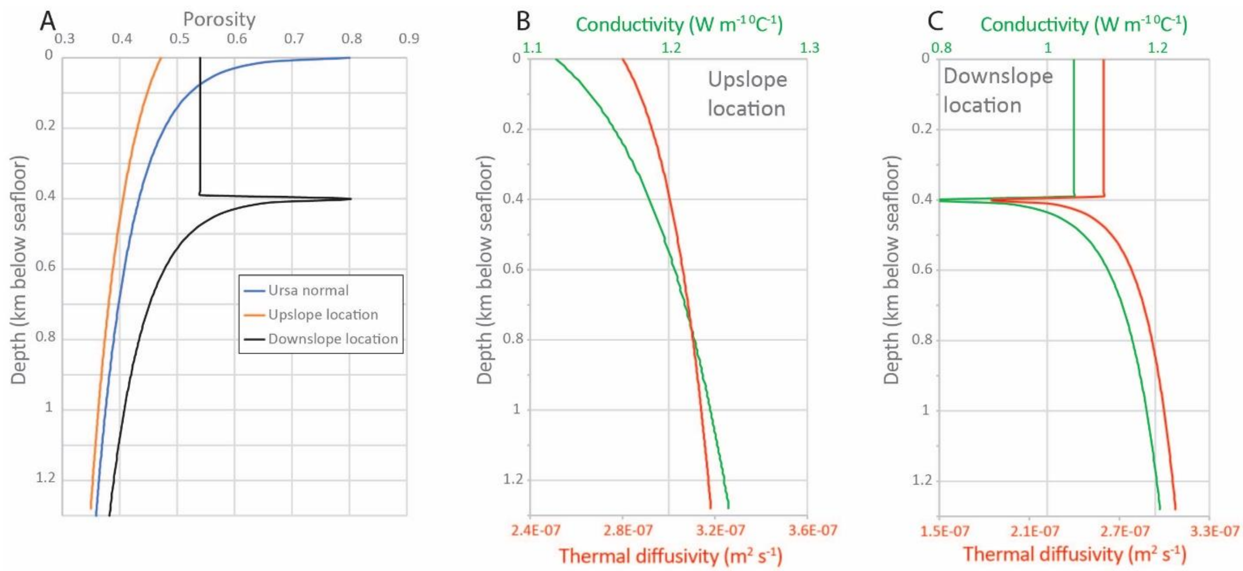

Supplementary Figure 3 A) Depth-porosity profiles used in the numerical 1D heat flow modeling at the upslope and downslope locations. B) Bulk thermal conductivity and thermal diffusivity profiles used at the upslope location C) Bulk thermal conductivity and thermal diffusivity profiles used at the downslope location.

Calculation of depth-porosity profiles

For the transient 1D heat flow model, we specify the porosity profile with depth using measured porosity from the Integrated Ocean Drilling Program Site U1324 in the Ursa Basin, Gulf of Mexico, approximately 260 km NE of the Orca Basin (Flemings et al., 2006) (blue in Supplementary Figure 3A). We use the Ursa Basin porosity profile to calculate the bulk thermal diffusivity and conductivity for the 1D models because it has higher resolution compared to the profile applied in the deep 2D heat flow modeling. Both, low- and high-resolution profiles are in a good agreement within the transient 1D heat flow model domain.

We assign a porosity profile at the upslope location (orange in Supplementary Figure 3A) to account for the 220 meters of sediment that was removed by the landslide. Therefore, the porosity starts from the normal Ursa porosity at 220 mbsf and we assume no elastic rebound. At the downslope site, we assign a porosity profile (black in Supplementary Figure 3A) to account for the addition of ~400 meters of landslide deposits on top of the pre-slide seafloor. We assume the MTD has a lower porosity typical of many MTDs worldwide, which is estimated to be the average porosity from 0-400 m at Ursa. Beneath the landslide mass, the porosity restarts similar to a seafloor profile, assuming negligible consolidation. The assumption of negligible consolidation results in 70-80% porosity within the upper ~10 m below the MTD. Such high porosity is unlikely because a ~400 m thick MTD would result in fast sediment consolidation soon after the slide event. However, we use this profile because such a narrow high-porosity interval below the MTD provides negligible effect on the modeling results.

Calculation of bulk heat capacity

The bulk heat capacity, C_{bulk}, (J kg^{-1} ^{o}C^{-1}) is calculated using:

$$C_{bulk} = (1-\phi)\rho_s C_s + \phi\rho_w C_w, \quad (2)$$

where ϕ is porosity, C_s and C_w are the specific heat capacity (J kg^{-1} ^{o}C^{-1}) of sediment and water, respectively, and ρ_s and ρ_w are the density (kg m^{-3}) of sediment and pore water, respectively (see Supplementary Table 1). The values for ρ_w depend on pressure, temperature and salinity (Fofonoff and Millard Jr, 1983).

Calculation of bulk thermal conductivity

The bulk thermal conductivity, $\lambda_{bulk,}$ (W m^{-1} ^{o}C^{-1}) is calculated using:

$$\lambda_{bulk} = (1-\phi)\lambda_s + \phi\lambda_w, \quad (3)$$

where λ_s and λ_w are the thermal conductivity (W m^{-1} ^{o}C^{-1}) of the sediment and pore water, respectively (see Supplementary Table 1).

Calculation of thermal diffusivity

The thermal diffusivity, κ (m^2 s^{-1}) is calculated using:

$$\kappa = \frac{\lambda_{bulk}}{C_{bulk}}, \quad (4)$$

From equations (2), (3), (4) we obtain the average thermal diffusivity of 3.0E-7 m^2 s^{-1} within our vertical model domain at Orca. This value was used for the Orca slide age estimate in the analytical approach (Figure 4, main text).

Supplementary Table 1. Parameters used for the transient 1D heat flow modeling.

Parameters	Values
Solid grain density (Dvorkin et al., 2000), ρ_s	2650 kg m^{-3}
Sediment specific heat capacity (Waples and Waples, 2004), C_s	1351 J kg^{-1} ^{o}C^{-1}
Pore water specific heat capacity (Waples and Waples, 2004), C_w	4208 J kg^{-1} ^{o}C^{-1}
Sediment heat conductivity (Class et al., 2002), λ_s	1.6 W m^{-1} ^{o}C^{-1}
Pore water heat conductivity (Class et al., 2002), λ_w	0.58 W m^{-1} ^{o}C^{-1}

Age estimation at the downslope location

The initial temperature profile within the MTD is somewhat ambiguous because slope failure is a chaotic process involving sediment redeposition and unpredictable rates of mixing with the cold bottom water. We select a uniform 7.5 °C temperature throughout the MTD for the model, which was the mean temperature in the ~220 m thick upslope sediment column prior to failure (supplementary Figure 4).

The model shows that at the downslope location the depth of the pre-slide BSR was 1120 mbsf (supplementary Figure 4). It will reach its complete post-slide steady-state depth at 680 mbsf, ~350 kyrs after the slide event. The modern BSR is observed in the seismic data at ~1090 mbsf, which is only 30 m above its pre-slide location (supplementary Figure 4). The modern BSR depth and methane phase boundary intersection corresponds to the ~14 kyr time-temperature profile (red line in supplementary Figure 4).

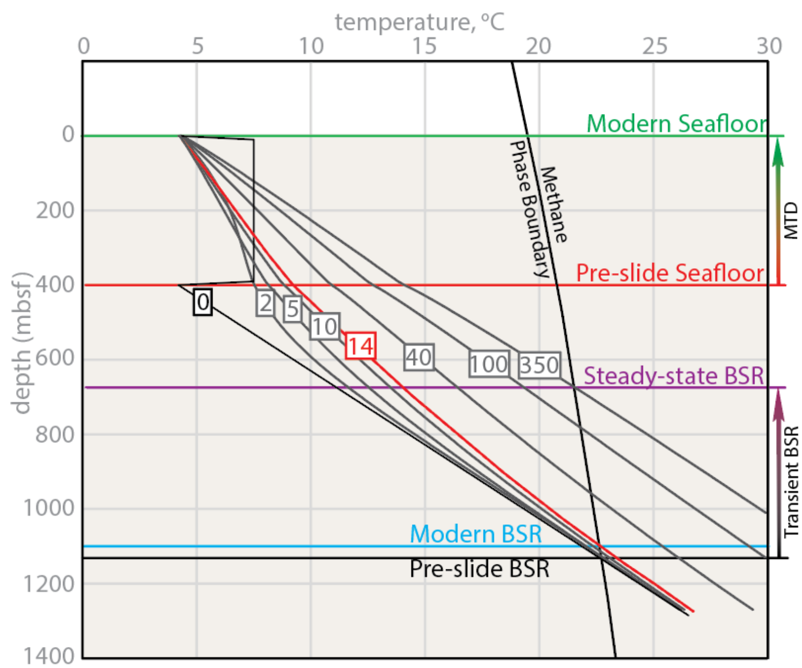

Supplementary Figure 4. Transient 1D heat flow modeling at the downslope location showing the time-temperature profiles after the addition of MTD assuming no gas hydrate dissociation. The model shows a 14 kyr age for the Orca landslide, which is likely less accurate than the upslope estimate (see main text for details).

2. Analytical solution below slide escarpments

For more general cases, it is possible to assume homogeneous sediment properties and a constant geothermal heat flux below the slide escarpments. By solving equation (1) with constant λ_{bulk} and C_{bulk} we obtain an analytical expression for the depth evolution of the GHSZ (z_{bsr}, m) with a known temperature at the BHSZ (T_{bsr}, °C) (Turcotte and Schubert, 2002):

$$\frac{T_{bsr}-T_{z,0}}{T_{s,1}-T_{s,0}} = erfc\left(\frac{z_{bsr}}{2\sqrt{\kappa t}}\right), \qquad (5)$$

where $T_{s,0}$ and $T_{s,1}$ are the seafloor temperature before and after the change, respectively (°C); $T_{z,0}$ is the initial temperature below the seafloor at depth *z* (°C) (Figure 4, main text); T_{bsr} can be derived from the modern BSR depth and methane hydrate phase boundary function with site-specific gas composition and salinity data. If the gas composition and salinity are unknown, for the most non-advective gas hydrate systems it is possible to assume a 100% methane gas and 3.5% pore-water salinity, and we follow these assumptions in our universal approach (Figure 4, main text); κ is the average thermal diffusivity of the subseafloor sediment (see "calculation of thermal diffusivity" chapter above); *t* is time (sec). To easily derive the input parameters and perform the analytical solution, we developed a desktop app for quick-look submarine landslide dating, which can be downloaded at www.portnovalexey.com (Supplementary Figure 5, 7).

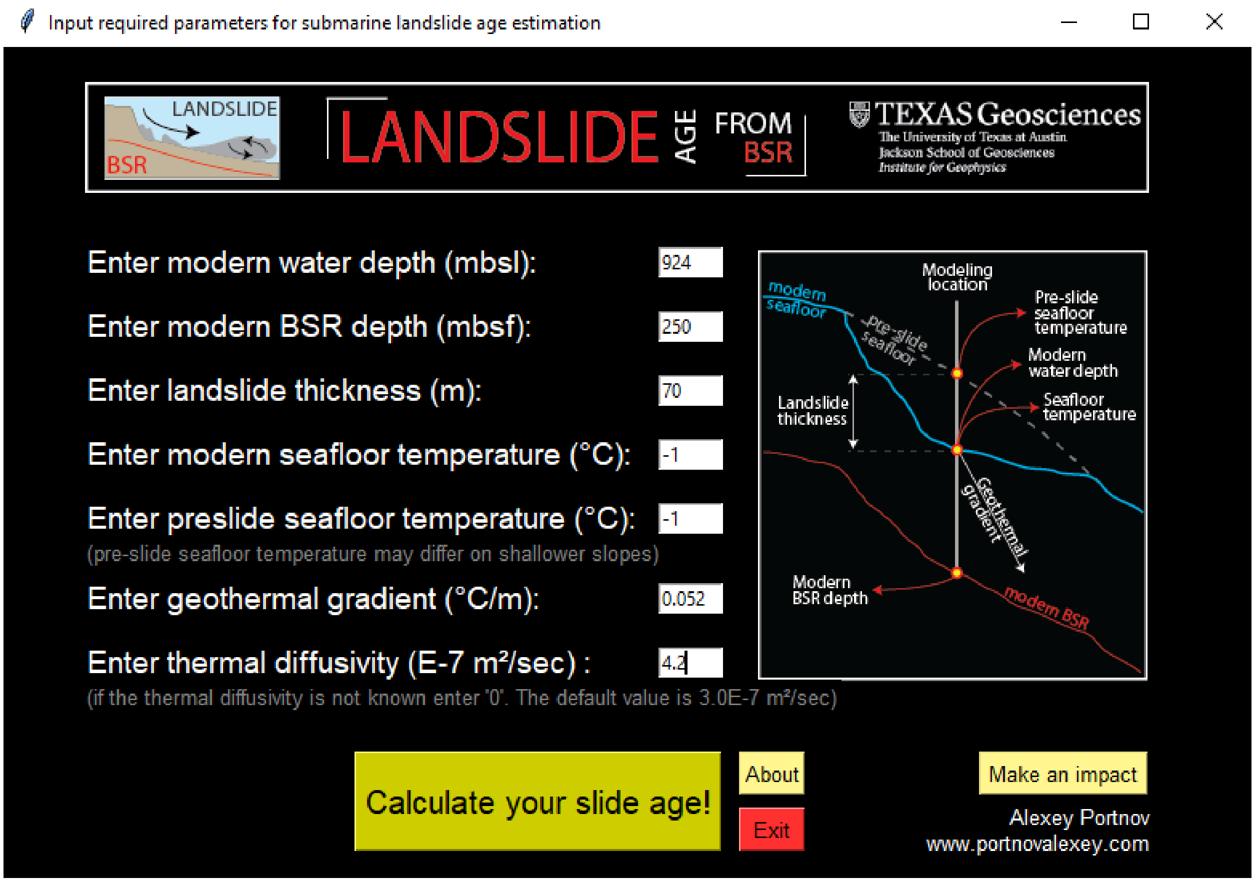

Supplementary Figure 5. Input interface of the desktop application for submarine landslide dating showing inputs used at the Storegga landslide (chapter 4).

3. Sensitivity of the BSR-based dating technique

The BSR-based submarine landslide dating technique is sensitive to the input parameters: BSR depth, landslide thickness, bottom water temperature, geothermal gradient, and thermal diffusivity. To demonstrate the sensitivity trends, we analyze three inputs to which the model is most sensitive: geothermal gradient, BSR depth and landslide thickness. We assume 100% methane gas for our sensitivity analyses.

Our analyzes show that the age uncertainty steadily increases with the increasing age of a landslide regardless of the model configuration. Supplementary Figure 6 shows sensitivity analyses for the model configuration similar to the Orca submarine landslide and includes various BSR depths corresponding to 1-32 kyr slide age range. As shown for the Orca landslide, a ±1 °C/km change in the geothermal gradient results in a ~±2 kyr of uncertainty, whereas 5-meter change in the BSR depth and 10-meter change in landslide thickness results in ~0.9 kyr age uncertainty. It is evident that constraining the geothermal gradient is of the prime importance especially for the older (>15 kyr) submarine landslides. At Orca, BSR depth and landslide thickness are less critical, yet, the significance of each input parameter depends on the particular system. For example, Supplementary Figure 6B shows Orca model configuration, but using a 50 °C/km geothermal gradient. In this case, the uncertainty associated with the geothermal gradient has less influence, but picking the precise BSR depth becomes more important.

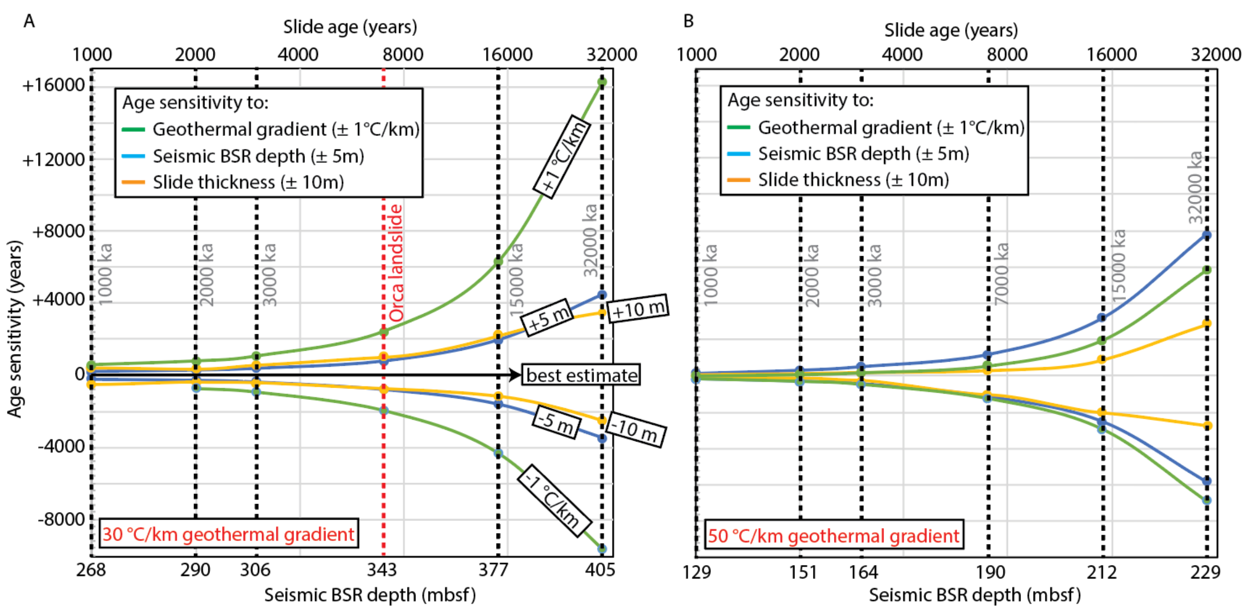

Supplementary Figure 6. We analyze model sensitivity to the geothermal gradient, the seismic BSR depth and the landslide thickness for submarine slides in the age range of 1-32 kyr using 30 °C/km (A) and 50 °C/km (B) geothermal gradients. The diagram in A shows that variation of the geothermal gradient (most critical parameter) within a 2 °C/km window results in ±2000 kyr age uncertainty for the Orca landslide age estimate.

4. Validation of the analytical approach at Storegga landslide

We validate the BSR-based dating method at the main Storegga landslide escarpment (Supplementary Figure 7A). The main Storegga landslide was a single event, which has been extensively studied and dated to ~8.1±0.25 ka using analyses of sediment cores and tsunami deposits (Haflidason et al., 2005). We use a 71-km long high-resolution seismic line acquired in 2000 by the UiT – The Arctic University of Norway (Mienert et al., 2005). We derive modern water depth (924 mbsl), modern BSR depth (250 mbsf), and landslide thickness (70 m) at the selected 1-D modeling location with an apparent BSR (Supplementary Figure 7A). Time-depth conversions were based on a measured velocity in the water column (1475 m/sec) and OBS-derived sediment velocity profile near the Storegga landslide (Plaza-Faverola et al., 2010). Based on the previous study of hydrate-bound gas at the nearby Nyegga pockmark field, gas shows microbial origin with the average 99.6% of methane, with trace amounts of higher-order hydrocarbons in the total gas composition (Vaular et al., 2010) (G11 pockmark). We use bottom water temperature (-1 °C), pre-slide seafloor profile and thermal diffusivity (4.2E-7 m^2/sec) based on the existing measurements at the Storegga landslide (Mienert et al., 2005). The measured geothermal gradients around Storegga are within the 50-55 °C/km range (Mienert et al., 2005). Using BSR depths outside the Storegga escarpment, we estimated the geothermal gradient at 52 °C/km near our modeling location (Supplementary Figure 6B). This geothermal gradient produces slide age of a ~8.1 ka, which is similar to the existing estimate (Haflidason et al., 2005). A geothermal gradient uncertainty of +1 and -1 °C/km will result in +4 and -2.5 kyr age uncertainty. Our dating at Storegga shows that with the well-constrained input parameters, BSR-based landslide dating method provides valid slide age estimates particularly for the relatively young (<15 ka) landslides.

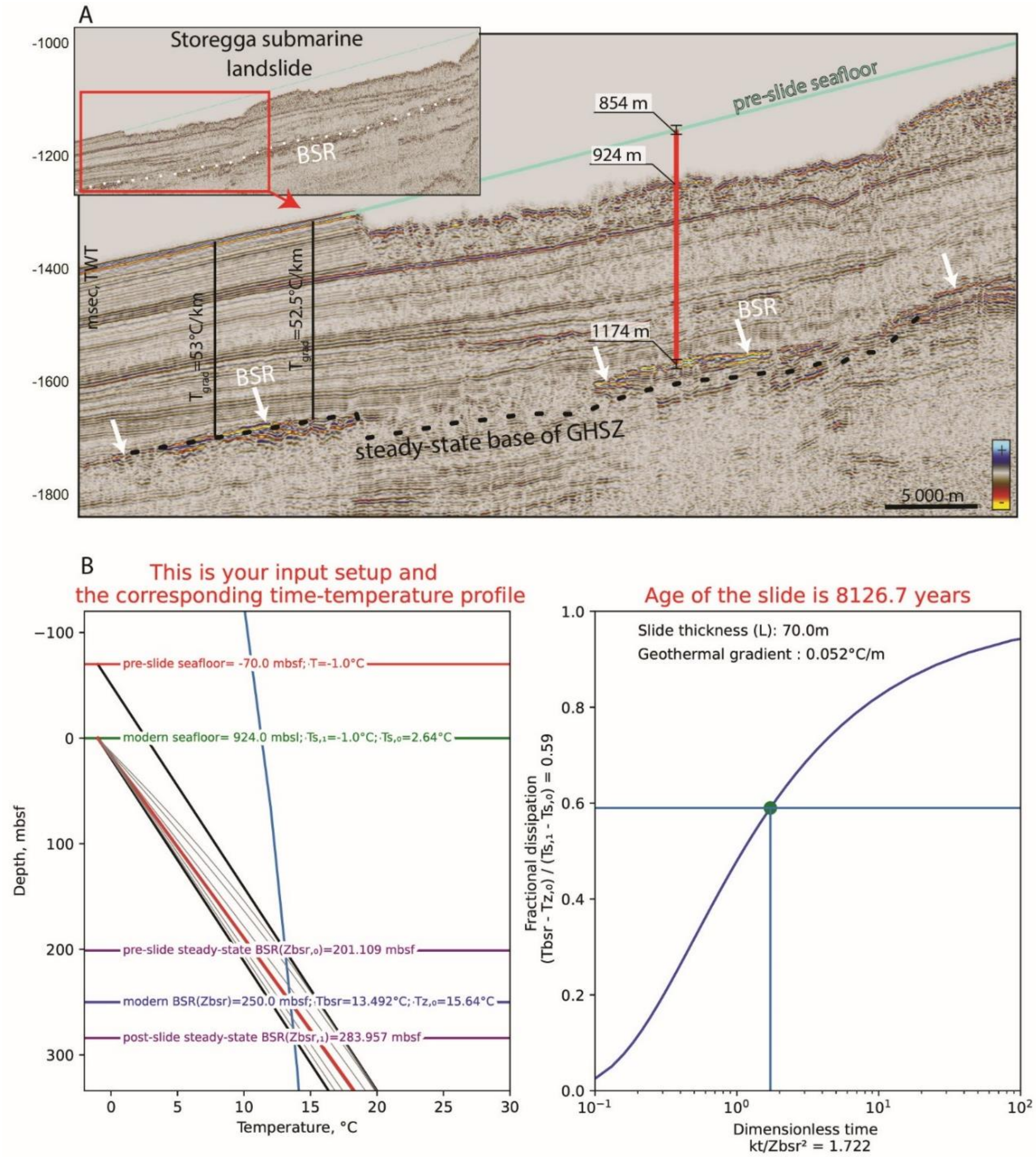

Supplementary Figure 7. (A) Reflection seismic profile JM00-026 (Mienert et al., 2005) crossing the Storegga slide headwall and its northern side wall. Red vertical line indicates the 1-D modeling location for slide age estimation. Pre-slide seafloor reconstruction, bottom water temperature (-1 °C), thermal diffusivity (4.2E-7 m^2/sec) and methane phase boundary are from the existing studies at the Storegga landslide (Mienert et al., 2005; Vaular et al., 2010). B) Analytical solution for the Storegga submarine landslide provides a ~8.1 ka slide age using 52

°C/km geothermal gradient, which is consistent with the existing analyses of sediment cores and tsunami deposits (Haflidason et al., 2005).

5. References

Bondevik, S., Løvholt, F., Harbitz, C., Mangerud, J., Dawson, A., and Svendsen, J.I., 2005, The Storegga Slide tsunami—comparing field observations with numerical simulations: Marine and Petroleum Geology, v. 22, p. 195–208, doi:10.1016/J.MARPETGEO.2004.10.003.

Christie, C.H., and Nagihara, S., 2016, Geothermal gradients of the northern continental shelf of the Gulf of Mexico: Geosphere, v. 12, p. 26–34, doi:10.1130/GES01163.1.

Class, H., Helmig, R., and Bastian, P., 2002, Numerical simulation of non-isothermal multiphase multicomponent processes in porous media.: 1. An efficient solution technique: Advances in Water Resources, v. 25, p. 533–550, doi:10.1016/S0309-1708(02)00014-3.

Dvorkin, J., Helgerud, M.B., Waite, W.F., Kirby, S.H., and Nur, A., 2000, Introduction to Physical Properties and Elasticity Models: , p. 245–260, doi:10.1007/978-94-011-4387-5_20.

Flemings, P.B., Behrmann, J.H., and John, C.M., 2006, Expedition 308 Scientists, Site U1324. Proc. IODP, 308: College Station TX (Integrated Ocean Drilling Program Management International, Inc.):, doi:10.2204/iodp.proc.308.108.2006.

Fofonoff, N.P., and Millard Jr, R.C., 1983, Algorithms for the computation of fundamental properties of seawater.:, doi:10.25607/OBP-1450.

Haflidason, H., Lien, R., Sejrup, H.P., Forsberg, C.F., and Bryn, P., 2005, The dating and morphometry of the Storegga Slide: Marine and Petroleum Geology, v. 22, p. 123–136, doi:10.1016/J.MARPETGEO.2004.10.008.

Herring, J., 2010, Gulf of Mexico Hydrographic Climatology and Method of Synthesizing Subsurface Profiles From the Satellite Sea Surface Height Anomaly:, https://geo.gcoos.org/data/ssha/ssha_ts_proflies.pdf.

Mello, U.T., Karner, G.D., and Anderson, R.N., 1995, Role of salt in restraining the maturation of subsalt source rocks: Marine and Petroleum Geology, v. 12, p. 697–716, doi:10.1016/0264-8172(95)93596-V.

Mienert, J., Vanneste, M., Bünz, S., Andreassen, K., Haflidason, H., and Sejrup, H.P., 2005, Ocean warming and gas hydrate stability on the mid-Norwegian margin at the Storegga Slide: Marine and Petroleum Geology, v. 22, p. 233–244, doi:http://dx.doi.org/10.1016/j.marpetgeo.2004.10.018.

Plaza-Faverola, A., Bünz, S., and Mienert, J., 2010, Fluid distributions inferred from P-wave velocity and reflection seismic amplitude anomalies beneath the Nyegga pockmark field of the mid-Norwegian margin: Marine and Petroleum Geology, v. 27, p. 46–60, doi:10.1016/J.MARPETGEO.2009.07.007.

Portnov, A., Cook, A.E., Sawyer, D.E., Yang, C., Hillman, J.I.T., and Waite, W.F., 2019, Clustered BSRs: evidence for gas hydrate-bearing turbidite complexes in folded regions, example from the Perdido Fold Belt, northern Gulf of Mexico: Earth and Planetary Science Letters,.

Sloan, E.D., and Koh, C.A., 2008, Clathrate Hydrates of Natural Gases, Third Edition: CRC Press, 752 p., doi:doi:10.1201/9781420008494.fmatt 10.1201/9781420008494.fmatt.

Turcotte, D.L., and Schubert, G., 2002, Geodynamics:, doi:10.1017/CBO9780511807442.

Vanneste, M., Harbitz, C., De Blasio, F., Glimsdal, S., Mienert, J., and Elverhøi, A., 2011, Hinlopen-Yermak landslide, Arctic Ocean—geomorphology, landslide dynamics and tsunami simulations: Mass-Transport Deposits in Deepwater Settings, edited by: Shipp, R., Weimer, P., and Posamentier, H, v. 96.

Vaular, E.N., Barth, T., and Haflidason, H., 2010, The geochemical characteristics of the hydrate-bound gases from the Nyegga pockmark field, Norwegian Sea: Organic Geochemistry, v. 41, p. 437–444, doi:10.1016/J.ORGGEOCHEM.2010.02.005.

Waples, D.W., and Waples, J.S., 2004, A Review and Evaluation of Specific Heat Capacities of Rocks, Minerals, and Subsurface Fluids. Part 1: Minerals and Nonporous Rocks: Natural Resources Research 2004 13:2, v. 13, p. 97–122, doi:10.1023/B:NARR.0000032647.41046.E7.

You, K., and Flemings, P.B., 2018, Methane Hydrate Formation in Thick Sandstones by Free Gas Flow: Journal of Geophysical Research: Solid Earth, v. 123, p. 4582–4600, doi:10.1029/2018JB015683.